www.nature.com/ismej

ISME

ARTICLE OPEN

Check for updates

# Marine picocyanobacterial PhnD1 shows specificity for various phosphorus sources but likely represents a constitutive inorganic phosphate transporter

Bhumika S. Shah[1,2]✉, Benjamin A. Ford[1], Deepa Varkey[1], Halina Mikolajek[3], Christian Orr[3], Vitaliy Mykhaylyk[3], Raymond J. Owens[4,5] and Ian T. Paulsen[1,2]✉



Despite being fundamental to multiple biological processes, phosphorus (P) availability in marine environments is often growth-limiting, with generally low surface concentrations. Picocyanobacteria strains encode a putative ABC-type phosphite/phosphate/phosphonate transporter, *phnDCE*, thought to provide access to an alternative phosphorus pool. This, however, is paradoxical given most picocyanobacterial strains lack known phosphite degradation or carbon-phosphate lyase pathway to utilise alternate phosphorus pools. To understand the function of the PhnDCE transport system and its ecological consequences, we characterised the PhnD1 binding proteins from four distinct marine *Synechococcus* isolates (CC9311, CC9605, MITS9220, and WH8102). We show the *Synechococcus* PhnD1 proteins selectively bind phosphorus compounds with a stronger affinity for phosphite than for phosphate or methyl phosphonate. However, based on our comprehensive ligand screening and growth experiments showing *Synechococcus* strains WH8102 and MITS9220 cannot utilise phosphite or methylphosphonate as a sole phosphorus source, we hypothesise that the picocyanobacterial PhnDCE transporter is a constitutively expressed, medium-affinity phosphate transporter, and the measured affinity of PhnD1 to phosphite or methyl phosphonate is fortuitous. Our MITS9220_PhnD1 structure explains the comparatively lower affinity of picocyanobacterial PhnD1 for phosphate, resulting from a more limited H-bond network. We propose two possible physiological roles for PhnD1. First, it could function in phospholipid recycling, working together with the predicted phospholipase, TesA, and alkaline phosphatase. Second, by having multiple transporters for P (PhnDCE and Pst), picocyanobacteria could balance the need for rapid transport during transient episodes of higher P availability in the environment, with the need for efficient P utilisation in typical phosphate-deplete conditions.

*The ISME Journal* (2023) 17:1040–1051; https://doi.org/10.1038/s41396-023-01417-w

## INTRODUCTION

Phosphorus (P) is an essential biological building block, integral for processes such as energy use (ATP), cell structure (phospholipids), and storage of genetic information in nucleic acids [1]. Dissolved P is also vital to the biogeochemistry of marine environments. The availability of the primary bioavailable form of P in its most oxidised state (+5), the inorganic phosphate ion ($P_i$), significantly influences the growth, abundance, and diversity of the most abundant photosynthetic microorganisms on Earth, marine picocyanobacteria of the genera *Prochlorococcus* and *Synechococcus* [2–4]. Low-nanomolar concentrations of $P_i$ have been reported in various marine environments, which could limit picocyanobacterial growth in these areas [5].

Marine picocyanobacteria have a well-characterised response to $P_i$ limitation [5–7], leading to significant alterations in gene expression, particularly of the phosphate regulation (*Pho* regulon) network. The nature and organisation of the *Pho* regulon is highly variable, even between related picocyanobacteria [7], corresponding to different adaptation strategies between different ecotypes [4, 6]. Genes encoding the high-affinity multicomponent periplasmic binding protein-dependent $P_i$ specific transporter (Pst) are shown to be significantly up-regulated under $P_i$ starvation in marine picocyanobacteria [7]. Marine picocyanobacterial genomes lack genes encoding the low-affinity constitutively expressed single-component $P_i$ symporter system (Pit) found in *E. coli* [4, 8, 9]. It is hypothesised that $P_i$ uptake via the Pit system could be energetically more favourable due to the symport with protons at 1:1 stoichiometry as opposed to $P_i$ uptake via the Pst system that potentially requires hydrolysis of two ATP per substrate transported [10].

Picocyanobacterial strains also encode a well-conserved predicted ABC-type phosphite/phosphate/phosphonate transporter, $PhnD_1CE$, which is thought to provide access to an alternative P pool such as organic phosphonates, Pn (P valence +3) or the inorganic reduced P compound phosphite, $P_t$ (P valence +3) [5]. The ability to uptake alternate P sources could provide significant competitive advantages under $P_i$-depleted conditions. Physiological studies on picocyanobacteria, however, demonstrate variability

[1]School of Natural Sciences, Macquarie University, Sydney, NSW, Australia. [2]ARC Centre of Excellence in Synthetic Biology, Macquarie University, Sydney, NSW, Australia. [3]Diamond Light Source Ltd., Harwell Science and Innovation Campus, Didcot, UK. [4]Division of Structural Biology, The Wellcome Centre for Human Genetics, University of Oxford, Oxford, UK. [5]Structural Biology, Rosalind Franklin Institute, Harwell Science and Innovation Campus, Didcot, UK. ✉email: bhumika.shah@mq.edu.au; ian.paulsen@mq.edu.au

Received: 22 November 2022 Revised: 14 March 2023 Accepted: 13 April 2023
Published online: 22 April 2023

in the expression of the $PhnD_1CE$ transport system under P stress. While some picocyanobacterial strains induce the expression of $PhnD_1CE$ transporter in a P-deficient media as shown for *Synechococcus* WH8102 [11], in some *Prochlorococcus* strains, it is not induced under P limitation [12] or can be constitutively expressed [11]. Several picocyanobacterial strains also encode an additional $PhnCD_2E$ transporter that clusters distinctly on protein phylogenetic trees [2, 3].

As the periplasmic substrate-binding component of the two predicted picocyanobacterial Pn transporters, PhnD1 and PhnD2, are typically co-expressed with the PhnC and PhnE components, the binding proteins have been used as proxies to investigate the substrate specificities of the respective transporter to understand their role in P acquisition [2, 3, 13]. Biophysical and structural data on PhnD1 and PhnD2, isolated from *Prochlorococcus* MIT9301, show diverse substrate specificity. While *Prochlorococcus* MIT9301_PhnD1 shows a high affinity for $P_t$ with a binding affinity ($K_D$) in the sub-micromolar range and comparatively weaker affinity to $P_i$ and methylphosphonate (MPn), *Prochlorococcus* PhnD2 show a stronger affinity for MPn followed by $P_t$ [2, 3, 13]. Unlike the *Prochlorococcus* PhnD proteins, there is a distinct lack of understanding regarding the specificity range of PhnD proteins within *Synechococcus* strains.

For various *Synechococcus* isolates, low P quotas and high uptake rates underscore the intense P competition in nutrient deplete oligotrophic environments [5, 14]. Low available P concentrations exert an intense selective pressure that influences the repertoire of P acquisition mechanisms of the related *Prochlorococcus* strains [12], most of which are also shared by *Synechococcus* isolates [5]. Several genes responsible for P acquisition have been acquired horizontally [12], indicating acquisition strategies between different strains likely reflect local P availability.

*Synechococcus* strains from clade I (e.g. CC9311) and IV generally co-occur in coastal and/or temperate mesotrophic open ocean waters, largely above 30°N and below 30°S [15, 16], alongside a broad nitrate and phosphate concentration range (0.03 to 14.5 µM and 0.2 to 1.2 µM, respectively) [5]. In contrast, *Synechococcus* clade II strains (e.g. CC9605) are abundant in coastal/continental shelves strictly in the subtropical/tropical latitudes (between 30°N and 30°S) [15–18]. *Synechococcus* clade III isolates (e.g. WH8102) do not show any latitudinal preference but are restricted to limited nitrate and phosphate concentrations [15], whereas clades CRD1 (e.g. MITS9220) and CRD2 are most successful in low Fe waters [19]. We examined PhnD1 from four marine *Synechococcus* strains (CC9311, CC9605, WH8102 and MITS9220) isolated from diverse environmental niches to characterise their corresponding ligand binding preferences and to explore the relationship between PhnD1 ligand specificity range and ecological niches.

## RESULTS AND DISCUSSION

### PhnD1 proteins in picocyanobacteria are lineage partitioned

The predicted phosphonate-binding protein (PhnD1) under study is found within the genome of all 97 sequenced picocyanobacteria strains in the Cyanorak database, comprising cluster CK_860 [20]. While the gene encoding PhnD1 is highly conserved among all picocyanobacterial genomes, our phylogenetic tree reveals it is distinctly partitioned by lineage, with *Prochlorococcus* representatives group separately from *Synechococcus* isolates and each clustering into clade-level groups (Fig. 1A). This highlights that the PhnD1 gene has been retained across evolutionary pressures and likely propagated by vertical transfer rather than horizontal gene transfer events. The latter is unlike the predicted duplicate copies, PhnD2 (cluster CK_6203; also annotated as PtxB [2, 3]) present in only a small number of strains (*Prochlorococcus* HLII/LLIV and *Synechococcus* clade II isolates) and a single PhnD3 (cluster CK_56876; only found in *Prochlorococcus* MIT9314) that cluster remotely from the PhnD1 genes. The low conservation of PhnD2 and PhnD3 indicates these are likely laterally transferred or results of lineage-specific gene duplications among ecotypes in similar environmental niches.

To evaluate the distribution and expression of PhnD1 and PhnD2 in marine picocyanobacterial populations, we investigated the metagenomes and metatranscriptomes available from the Ocean Microbial Reference Gene Catalogue (OM-RGC) [21, 22]. For comparison, we provide distribution maps for *Synechococcus* and *Prochlorococcus* lineage-specific genes (Supplementary Fig. S1A, B). This analysis revealed that picocyanobacterial PhnD1 transcripts (Fig. 1B) and genes (Supplementary Fig. S1C, D) are not only enriched in mostly $P_i$-replete waters but also some $P_i$-deplete areas across several Pacific Ocean, Atlantic Ocean and Indian Ocean sites (surface water as well as the deep chlorophyll maximum zone). In contrast, picocyanobacterial PhnD2 homologues were most abundant in $P_i$-limited surface waters in the North-western Atlantic Ocean, the Mediterranean Sea and the Gulf of Mexico.

Previous studies show that *Prochlorococcus* MIT9301, which encodes both *phnD1* and *phnD2*, can use $P_t$ or MPn as the sole P source to support its growth [2, 3, 23]. The ability of *Prochlorococcus* MIT9301 to grow on $P_t$ or MPn is attributed to the predicted phosphonate oxidative pathway encoded by the putative *phnY* (cluster CK_55307) and *phnZ* (cluster CK_7402) genes [23, 24] and a NAD-dependent phosphite dehydrogenase *ptxD* (cluster CK_56808), respectively. These predicted Pn and $P_t$ utilisation genes are co-located with the $phnC_2D_2E_2$ (also annotated as *ptxABC*) transport system in some picocyanobacterial strains. Based on these observations, we hypothesise that, by extension, all picocyanobacterial isolates encoding the $phnC_2D_2E_2$ and the adjacent *phnY*, *phnZ* and *ptxD* genes have the potential to metabolise $P_t$ or MPn, providing an ecological advantage to survive in a $P_i$-depleted environment. Our comparative genome analysis reveals *Prochlorococcus* and *Synechococcus* genomes sequenced to date, however, lack the *phnY*, *phnZ* and *ptxD* genes, suggesting these strains may not be able to utilise $P_t$ or MPn.

Based on the in vitro studies showing a very high affinity of *Prochlorococcus* MIT9301 PhnD1 to $P_t$ [3, 13], it is predicted that the transporter encoded by $phnD_1C_1E_1$ could be a phosphite transporter. However, studies show that *Prochlorococcus* strains MIT9313 and MED4 (lacking the $phnC_2D_2E_2$ transport system and the adjacent metabolising genes) are unable to grow and utilise $P_t$ (or MPn) and instead are only able to utilise $P_i$ for their growth [2, 3, 23]. Other studies examining the P-starvation response in picocyanobacteria indicate none of the components of the $phnD_1C_1E_1$ transport system showed any significant upregulation in P-deplete conditions, as opposed to the strong induction of genes previously implicated in P-scavenging, such as the high-affinity *pstS* gene [7, 12].

We examined the $phnD_1C_1E_1$ genome context and find a highly conserved gene (*tesA*; cluster CK_171), encoding a predicted lysophospholipase L1-like esterase, co-located in almost all picocyanobacterial sequenced genomes. While the function of the periplasmic TesA in picocyanobacteria is unclear, it has been previously proposed to be part of a complex enzymatic system responsible for phospholipid membrane homeostasis in *P. aeruginosa* [25]. Picocyanobacteria (*Prochlorococcus* MED4 and *Synechococcus* WH8102, WH7803, WH5701*)* are shown to have the ability to substitute sulfolipids for phospholipids in their membrane to economise P utilisation under P-limitation [26]. The same study also showed that while the "substitute lipids" are dominant in the P-limited cultures, the phospholipid substitution occurred in all cases, including in the P-replete conditions, although to a much smaller extent. The genes required for sulfolipid biosynthesis, *sqdB* (cluster CK_123) and *sqdX (*cluster CK_333), are conserved in all sequenced picocyanobacterial genomes and not just those abundant in the P-deplete conditions. It remains unclear if the conservation of sulfolipid biosynthesis genes (*sqdB, sqdX*) and the co-localisation of the $phnD_1C_1E_1$ transporter with conserved *tesA*

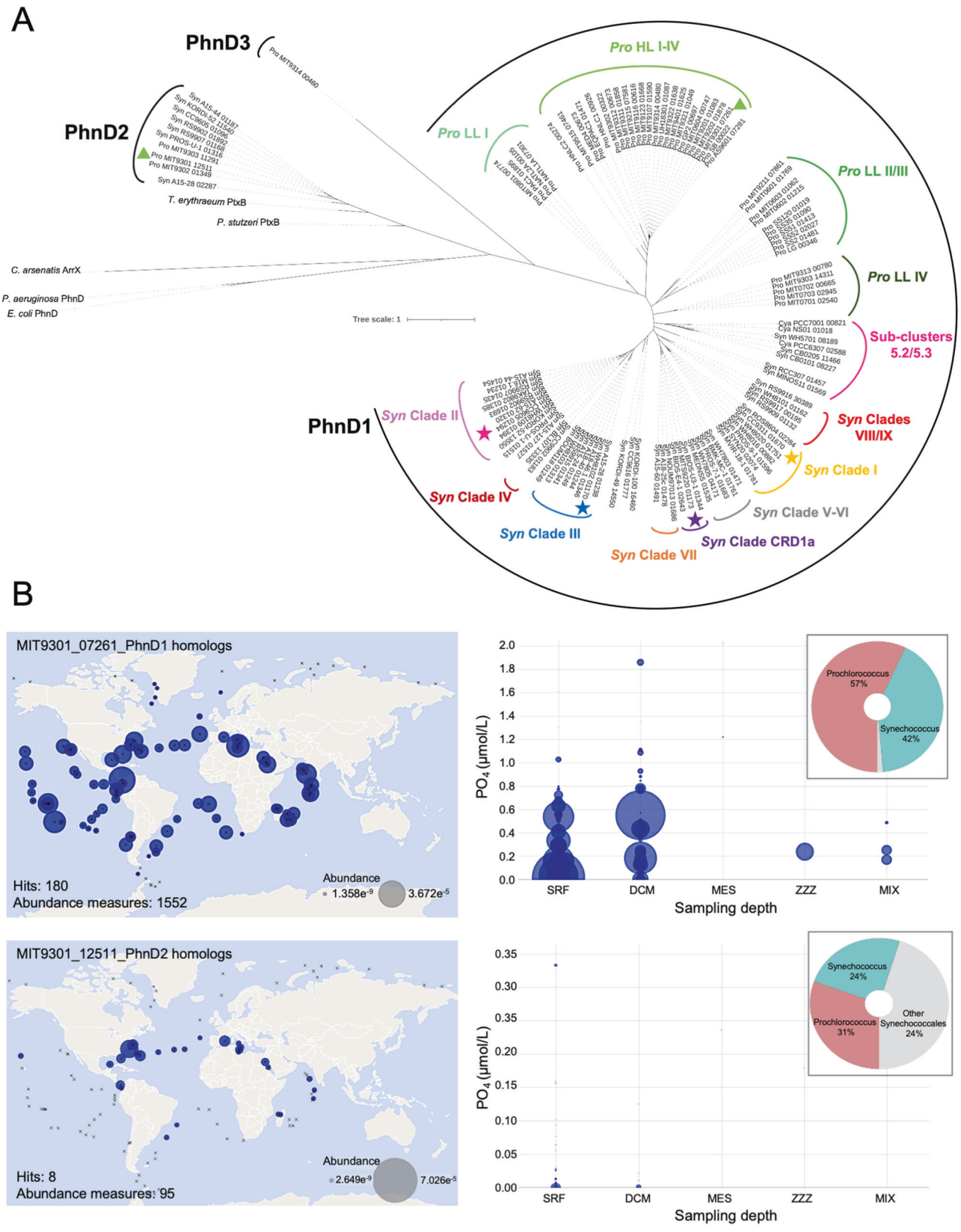


are correlated and what physiological advantage in terms of P utilisation this would provide to the marine picocyanobacterial strains. It is possible that TesA could play a role in breaking down phospholipids found in picocyanobacteria, such as the prevalent phosphatidylglycerol (PG). While the specific breakdown products of PG in cyanobacteria are currently unknown, in yeast, PG can be degraded to diacylglycerol and glycerol-3-phosphate (G3P) [27]. In this case, alkaline phosphatase could then cleave the phosphoryl group from the glycerol-3-phosphate, producing glycerol and inorganic phosphate ($P_i$), which could be taken up by the PhnDCE

**Fig. 1 Phylogenetic and genomic analyses of picocyanobacterial PhnD1 sequences. A** The amino acid sequences of *Synechococcus (Syn)* and *Prochlorococcus (Pro)* PhnD1 (CK_860), PhnD2 (CK_6203) and PhnD3 (CK_56876), as well as previously characterised non-picocyanobacterial PhnD proteins were aligned using MAFFT [40], and the phylogenetic tree inferred using IQ-Tree [41]. The final phylogenetic tree was visualised using iTOL [42]. The four *Synechococcus* PhnD1 proteins (CC9311, CC9605, WH8102 and CRD1a) characterised in this study are highlighted on the tree. Genes are numbered according to their Cyanorak cluster designation [20]. **B** The environmental abundance for *Prochlorococcus* MIT9301_PhnD1 (top-left) and MIT9301_PhnD2 (bottom-left) picocyanobacterial homologues extracted from the Tara Oceans MetaT dataset [57]. The transcript abundance is plotted for surface waters, with a circle size corresponding to the measured abundance at a particular sampling site. Sampling sites are denoted by an 'X'. The corresponding bubble plot (right) for the identified transcripts across sampling depths (SRF, surface waters; DCM, deep chlorophyll maximum; MES, mesopelagic zone; MIX, marine epipelagic mixed layers;) is depicted as a function of measured phosphate concentration. The Krona plot in the inset shows the taxonomic distribution of MIT9301_PhnD1, and MIT9301_PhnD2 homologues selected to analyse the metatranscriptome abundance.

or Pst transport system, setting the stage for a constant phosphorus supply irrespective of the environmental conditions.

### *Synechococcus* PhnD1 proteins show a preferential binding affinity for phosphite, phosphate and methylphosphonate

Several studies have examined the P-binding specificities for different PhnD proteins in *Prochlorococcus* [2, 3, 13]. This is the first study to report the substrate specificity range of *Synechococcus* PhnD1 proteins. We expressed and purified four *Synechococcus* PhnD1 proteins (CC9311_PhnD1, CC9605_PhnD1, MITS9220_PhnD1 and WH8102_PhnD1; Supplementary Fig. S2) and evaluated their potential ligand binding preferences by differential scanning fluorimetry (DSF). This was done by measuring the increase in melting temperature ($T_M$) of the protein in the presence of potential ligands. The first-pass ligand screen encompassed compounds (Supplementary Table S1), including a diverse range of biologically active small molecules, trace metals, and common metabolic nutrients (C, N, S, P sources) as well as inorganic phosphate ($P_i$), phosphite ($P_t$), methylphosphonate (MPn), and hypophosphite ($HP_t$). This comprehensive DSF screen reveals (Fig. 2A) all four PhnD1 proteins have higher thermal stability ($\Delta T_M$ 5–23 °C) only in cocktail conditions comprising P sources. Among the single P-sources tested, the most significant shift in the $T_M$ is observed in the presence of $P_t$ ($\Delta T_M$ 17–23 °C), followed by $P_i$ ($\Delta T_M$ 3–8 °C). A second DSF screen comprising 60 distinct individual P-sources were tested for CC9605_PhnD1 protein, including those representing the hydrophilic polar headgroups of various phospholipids such as 3-phospho glyceric acid, phosphoryl choline, inositol phosphate and phosphoserine (Supplementary Fig. S3). With the exception of carbamyl phosphate and phospho glycolic acid, which may act as a phosphate proxy due to their comparatively smaller size, no other phosphorous sources showed a marked increase in the thermal stability, indicating they are unlikely to be PhnD1 substrates.

A fluorometric isothermal approach [28, 29] was further utilised to determine the binding dissociation constants ($K_D$) of the four *Synechococcus* PhnD1 proteins in the presence of $P_i$, $P_t$, MPn, and $HP_t$ (Fig. 2B). This approach involves measuring incremental changes in the thermal stability (Supplementary Figs. S4–S7) caused by the partial formation of protein-ligand complexes, measured by an extrinsic dye [28, 29]. All four *Synechococcus* PhnD1 proteins displayed an affinity for at least two P sources: $P_i$ and $P_t$ (Fig. 2B); however, the specific binding affinities for these differ between each strain, as summarised in Table 1. Of the four proteins under study, MITS9220_PhnD1 displayed a comparatively stronger affinity for $P_t$ and $P_i$. The derived $K_D$ value for $P_t$ is at least an order of magnitude stronger than $P_i$ for each PhnD1 protein, indicating a markedly stronger affinity for $P_t$. This is intriguing, given the fact that most strains of picocyanobacteria lack known $P_t$ utilisation proteins.

Except for the CC9311_PhnD1, isolated from the strain found in the mesotrophic marine settings, three *Synechococcus* PhnD1 proteins also show a measurable affinity for MPn: CC9605_PhnD1 (17 ± 3 μM), WH8102_PhnD1 (41 ± 5 μM), and MITS9220_PhnD1 (47 ± 9 μM). While the binding affinity of these PhnD1 proteins for MPn is comparatively weaker than $P_i$ and $P_t$, the measured binding constants are comparable to that known for the *Prochlorococcus* MIT9301 PhnD1 homologue (Pm_PhnD1, $K_D = 39–108$ μM) (21). As organic phosphonates arise from cellular components, such as phospholipids, nucleic acids, amino acids, and polysaccharides, this broad substrate affinity observed for some *Synechococcus* isolates could potentially reflect an ability to access more labile forms of phosphorus [3, 30] rather than solely inorganic sources, which are generally sparingly soluble. As discussed earlier, none of the four Synechococcus strains under study (CC9311, CC9605, WH8102, MITS9220) harbours currently known putative $P_t$ or MPn utilisation genes (*ptxD, phnY/phnZ* or C-P lyase) in their genome. Therefore, the affinity of *Synechococcus* PhnD1 proteins to $P_t$ or MPn, analogous to the *Prochlorococcus* PhnD1 [3, 13], may be incidental, requiring further investigations into the structural mechanism of P selectivity for picocyanobacterial PhnD1 proteins.

### The crystal structure of MITS9220_PhnD1 in complex with phosphate reveals an extensive hydrogen bond network

While crystal structures of PhnD1 in complex with $P_t$ and MPn from *Prochlorococcus* are available, there are no crystal structures of picocyanobacterial PhnD1 protein in complex with $P_i$. Therefore, to understand the molecular mechanism of $P_i$ selectivity, we determined a high-resolution crystal structure (2.0 Å) of *Synechococcus* MITS9220_PhnD1 with bound $P_i$, resulting in a closed ligand-bound complex (Fig. 3). Data collection and final refinement statistics for the crystal structure are outlined in Table 2. The overall structure of MITS9220_PhnD1 is similar to that of other class II substrate binding proteins (SBPs) [31] and specifically to cluster-F SBPs [32, 33], with two α/β domains separated by a longer central hinge region (8–10 amino acids). The extended hinge region in cluster-F SBPs is believed to provide greater flexibility between the ligand-bound (closed) and unbound (open) conformations of cluster-F SBPs [33]. This hinge region encompasses a buried ligand-binding cavity and includes a $P_i$ molecule within the MITS9220_PhnD1 structure copurified with the protein. The MITS9220_PhnD1 structure displays an unusual asymmetric distribution of electrostatic surface potential (Fig. 3B), where the front is completely enveloped by positive charge, attracting several $Cl^-$ anions from the crystallisation buffer. While the presence of $Cl^-$ on the surface might be a crystallisation artifact, the strong positively charged front may have functional significance in facilitating picocyanobacterial PhnD1 association with the predominantly negatively charged phospholipid membrane surface.

Even though clear electron density is observed in the substrate binding site, which appears to have a tetrahedral geometry consistent with the $P_i$ molecule in the binding pocket (Fig. 3), all ligands under study ($P_i$, $P_t$, and MPn) have similar chemical structures. Therefore, careful assignment of $P_i$ to the positive difference Fourier electron density was ensured by considering van der Waals contacts and hydrogen bonds in the most appropriate chemical orientation and comparing refinements with the $P_i$ replaced by $P_t$ and MPn (Supplementary Fig. S8). Additionally, we also collected X-ray data above (2550 eV) and below (2400 eV) the sulphur edge, which assisted in dismissing the remote possibility of a sulphate ion instead being sequestered within the binding cavity (Supplementary Fig. S9).

Within the crystal structure of MITS9220_PhnD1, the four $P_i$ oxygens are bound by a total of 10 direct hydrogen bonds, forming an extensive H-bond network to the main chain and sidechains of

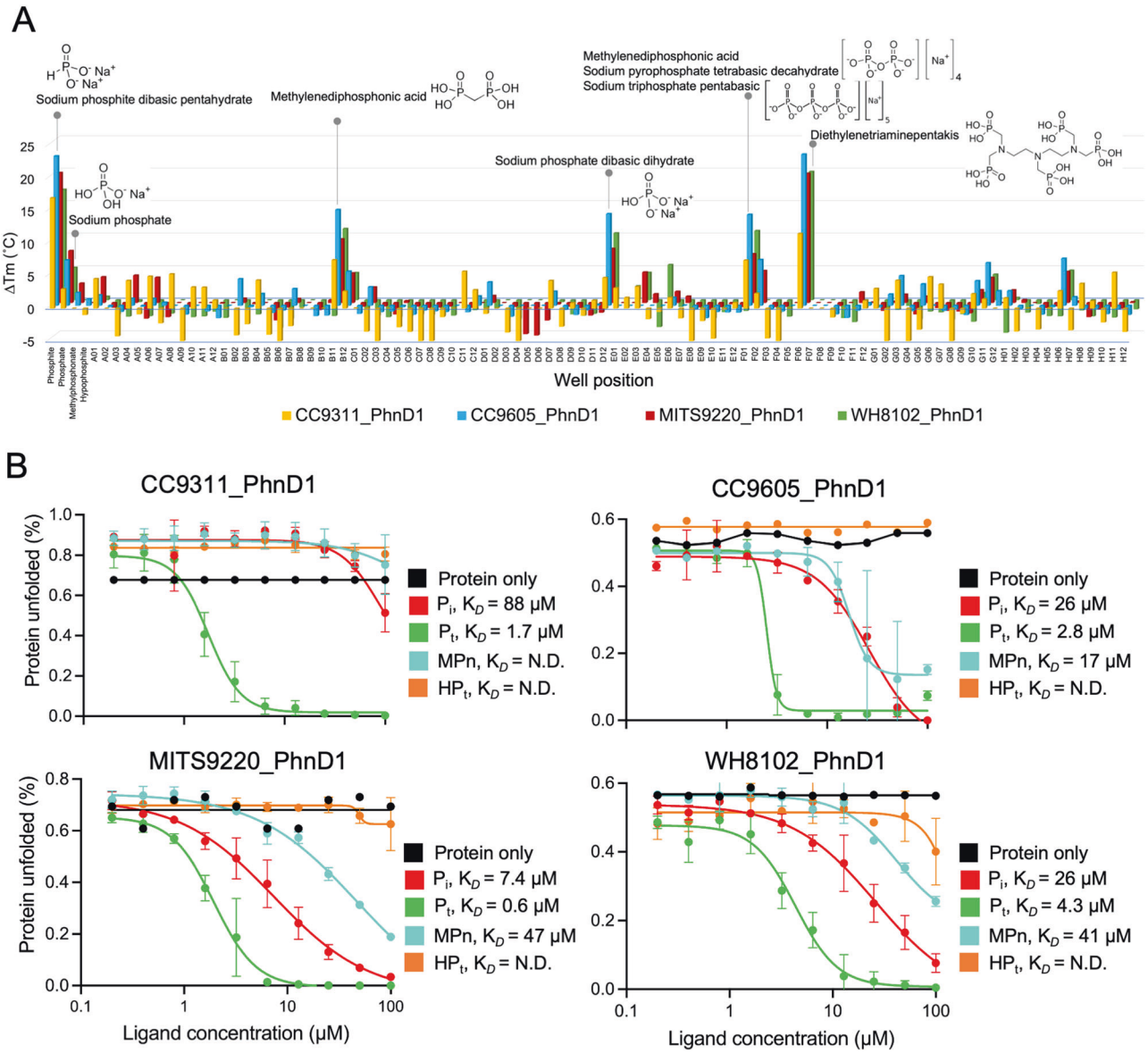


**Fig. 2 Ligand screening and binding affinity measurement of *Synechococcus* PhnD1 proteins. A** DSF thermal melt assay was used to screen ligands for CC9311_PhnD1 (yellow), CC9605_PhnD1 (blue), MITS9220_PhnD1 (red) and WH8102_PhnD1 (green) proteins in the presence of a range of cocktail solutions (Silver Bullets 96-well screen) containing unique biologically relevant potential substrates as well as with various P sources ($P_i$, $P_t$, MPn and $HP_t$). These data show that significant change in the melting temperature ($\Delta T_M$) is conferred only in cocktail conditions comprising P sources. **B** The measured binding affinity of the four *Synechococcus* PhnD1 proteins calculated based on the isothermal analysis of the DSF data (Supplementary Figs. S4–S7) upon incremental addition of the respective ligand; $P_i$ (red), $P_t$ (green), MPn (blue) or $HP_t$ (orange) is depicted. Reported affinities were computed using the Python package [29] and plotted on GraphPad Prism.

residues distributed between the two domains (Fig. 3A). These include a tyrosine (Y44) at the beginning of α2; an -STS- motif (S124, T125, S126) in a loop region joining β6 and α4; a histidine (H156) at the beginning of α6; an H-acceptor aspartic acid (D203) and a capping tyrosine residue (Y204) found just before β10. A single water molecule buried deep within the cavity also contributes to this hydrogen bond network. This water molecule is further stabilised by intramolecular hydrogen bonds to residues on domain 1 (T65) and domain 2 (S123), contributing to the interactions that connect the two domains and occluding the binding pocket from the solvent. Similarly, the capping Y204 sidechain is engaged in hydrogen bonds to residues D11 (domain 1) and N174 (domain 2), contributing to the two-domain interactions.

Sequence analysis shows strong conservation of all key MITS9220_PhnD1 $P_i$ binding residues among most picocyanobacteria PhnD1 homologues (Fig. 3C), suggesting an analogous $P_i$ binding mechanism in these isolates. The only exception is a substitution of aspartic acid (D203) to a functional homologue asparagine residue in the three Cyanobium strains, all *Prochlorococcus* LL1 strains (MIT0901, NatL1A, NatL2A, PAC1), and most *Synechococcus* clade I strains (Syn MV1R-18, Syn20, Pros 9-1, WH8016, WH8020) available on the Cyanorak database. In the absence of the biophysical data, it is unclear if the Asp to Asn substitution at the binding site impacts the P specificity of PhnD1 in these isolates, given the essential role of D203 as an H-bond acceptor.

### MITS9220_PhnD1 structural comparison reveals the molecular basis of broad P specificity and medium $P_i$ affinity

A search for structural homologues using the Dali server [34] reveals many structures similar to MITS9220_PhnD1 bound to $P_i$ (Table 3).

**Table 1.** Dissociation constants for *Synechococcus* PhnD1 proteins and their homologues.

| Protein | Strain | Gene ID | Clade | Ecological conditions | $P_i$[a] (μM) | $P_t$[a,b] (μM) | MPn[a] (μM) | 2-AEP[a,b] (μM) | Affinity measurement | Ref. |
|---|---|---|---|---|---|---|---|---|---|---|
| CC9311_PhnD1 | *Syn sp.* CC9311 | 01670 | I | Coastal and/or temperate mesotrophic open ocean [19] | 88 ± 20 | 1.7 ± 0.9 | – | *NM* | nanoDSF | Our study |
| CC9605_PhnD1 | *Syn sp.* CC9605 | 01294 | II | Offshore, oligotrophic tropical or subtropical waters [19] | 26 ± 10 | 2.8 ± 2 | 17 ± 3 | *NM* | nanoDSF | |
| MIT9220_PhnD1 | *Syn sp.* MITS9220 | 01173 | CRD1a | Low iron, high nutrient equatorial upwelling regions [58, 59] | 7.4 ± 1.3 | 0.67 ± 0.1 | 47 ± 9 | *NM* | nanoDSF | |
| WH8102_PhnD1 | *Syn sp.* WH8102 | 01170 | III | Ultraoligotrophic open-ocean waters [19] | 26 ± 8 | 4.3 ± 0.5 | 41 ± 5 | *NM* | nanoDSF | |
| Pm_PhnD1 | *Pro.* MIT9301 | 07261 | HLII | Strongly stratified surface waters, mainly tropical and subtropical regions [60] | 54.9 | 0.12 | 39.0 | – | ITC | [3] |
| | | | | | 182 ± 26 | 0.051 ± 0.004 | 109 ± 8 | – | Microscale thermophoresis | [13] |
| Pm_PtxB[c] | *Pro.* MIT9301 | 12511 | HLII | Strongly stratified surface waters, mainly tropical and subtropical regions [60] | – | 2.0 | 0.8 | – | ITC | [3] |
| Ec_PhnD | *E. coli* UTI89 | C4699 | n/a | n/a | 50 | *NM* | 1.3 | <0.05 | Intrinsic fluorescence | [61] |
| | | | | | – | – | 18.4 | 0.1 | ITC | [3] |

[a] *NM* denotes binding not measured.
[b] Dash indicates binding not detected in the respective study.
[c] PtxB is annotated as PhnD2 in the cyanorak database.

Among them, the structure of Pm_PhnD1 (56% sequence identity) in complex with $P_t$ and MPn is most similar to MITS9220_PhnD1, with an r.m.s.d. of 1.1 Å. The structure of Pm_PhnD2 in complex with $P_t$, sequence identity of 30% to MITS9220_PhnD1, is the second closest structural homologue (r.m.s.d 1.7 Å). In comparison, the *E. coli* PhnD structure differs markedly with an r.m.s.d. of 2.4 Å, whereas the high-affinity $P_i$-binding PstS protein in *E. coli* aligns distantly with an r.m.s.d. of 5.1 Å. The overall fold of *Synechococcus* MITS9220_PhnD1 (with $P_i$) structure and the close structural homologues from *Prochlorococcus* MIT9301 [13] are very similar (Fig. 4A). The chemical structure of $P_i$, $P_t$, and MPn only differs at the R1 position substituted by OH, H and $CH_3$, respectively. In all these structures, the R1 position of the respective P-ligand is capped by a tyrosine residue (Fig. 4B–D), leading to a smaller binding pocket for picocyanobacterial PhnD1 and PhnD2 proteins. In contrast, the *E. coli* PhnD (Ec_PhnD) crystal structure shows two H-bond acceptors, D205 and E177, in the active site, resulting in a comparatively larger binding cavity that can accommodate bulkier phosphonates, such as 2-aminoethylphosphonate (2-AEP) (Fig. 4E). The structural comparisons thus reveal the significance of the capping tyrosine residue as a steric barrier and rationalise why picocyanobacterial strains in the past were unable to bind and metabolise large complex Pn, such as 2-AEP [2, 23] but instead only use simple phosphonates such as MPn as a sole P source in strains encoding the potential Pn utilisation genes (*phnY/phnZ*) [23].

As discussed earlier, the $P_i$ in MITS9220_PhnD1 structure is co-ordinated by ten hydrogen bonds (Fig. 4B), where the three oxygen atoms are engaged in multiple H-bonds, three each with O1, O3 and O4 in a trigonal geometry. The O2 atom (representing the R1 group) is, however, stabilised by a single H-bond formed by the capping residue Y204 (Supplementary Table S3). In contrast, the crystal structures of the high-affinity $P_i$-specific binding protein PstS, for example, in *E. coli* (PDB 2ABH), show an extensive hydrogen bond network [35, 36] consisting of 14 H-bonds (Fig. 4F). In addition to the three oxygen atoms O1, O3 and O4 engaging in three H-bonds each, the O2 atom in the case of *E. coli* PstS is stabilised by five H-bonds in a pentagonal geometry, explaining the high-affinity and specificity of PstS to $P_i$. The comparison of the binding pocket of the medium and high-affinity $P_i$ binding proteins, MITS9220_PhnD1 and *E. coli* PstS, respectively, highlights the central role of the H-bond network in determining the specificity and binding affinity of the P-ligands. Our structural comparisons thus provide molecular insights into the potential fortuitous binding of $P_t$ or MPn and the comparatively lower affinity of picocyanobacterial PhnD1 to $P_i$.

Low-affinity substrate-binding proteins are better suited for rapid substrate turnover, while high-affinity substrate-binding proteins are well suited for substrate scavenging at low concentrations. By having multiple nutrient transporters with different binding affinities and transport rates, cells can mitigate a "rate-affinity trade-off" and ensure the efficient transport of nutrients under different conditions [37]. In picocyanobacteria, the high-affinity Pst transporter could therefore be used to maintain a steady supply of $P_i$ under phosphate-deplete conditions, while the comparatively low-affinity Phn transporter with potentially fast transport rates could be used to import large amounts of $P_i$ when it is transiently available. For example, in times of upwelling, riverine inputs or $P_i$ bursts from plankton or viral lysis. This would thus allow the picocyanobacterial cells to balance the need for rapid transport of nutrients under occasional conditions of plenty, with the need to efficiently utilise available P resources under typical phosphate-deplete conditions.

### *Synechococcus* strains MITS9220 and WH8102 do not utilise $P_t$ and MPn for growth as the sole P source

To test if *Synechococcus* strains not encoding *phnD2* and the adjacent $P_t$/Pn utilisation genes can use alternative P sources other than $P_i$, we examined their growth in culture conditions

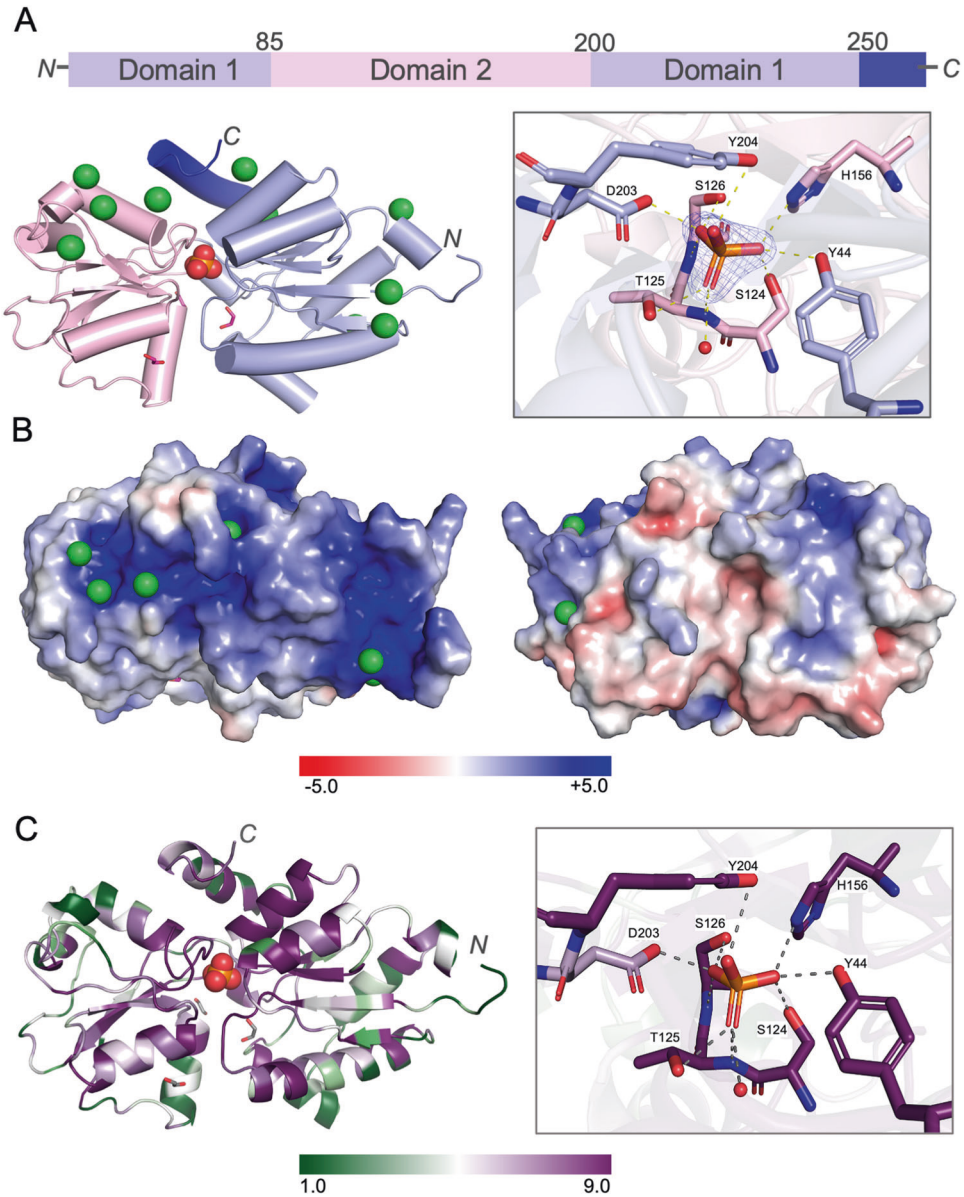


**Fig. 3 Crystal structure of MITS9220_PhnD1 in complex with phosphate. A** Block diagram representation (top) of the primary structure of MITS9220_PhnD1 showing the two lobes and the amino acids that determine the border of each domain. A cartoon representation (bottom-left) of the overall fold of MITS9220_PhnD1 highlighting the two α/β domains; lobe 1 (violet) and lobe 2 (pink), with $P_i$ drawn as spheres (red). Also included in the representation are ten $Cl^-$ ions (green spheres) and 3 EDO (magenta sticks) molecules sequestered from the crystallisation condition. A detailed view of the ligand-binding pocket (bottom-right), outlining the interactions between $P_i$ and MITS9220_PhnD1. The interacting sidechains and $P_i$ are shown as sticks and coloured as per the respective domains, with the protein backbone shown as a cartoon. The single buried water is shown as a red sphere. **B** The electrostatic surface potential of the front (left) and back (right) of the MITS_9220 PhnD1 structure, with positive (blue) and negative charge (red) shown. **C** The protein sequence conservation mapping of picocyanobacterial PhnD1 homologues on MITS9220_PhnD1 structure (left) and ligand-binding pocket (right). The areas with high conservation (purple) and low conservation (green) are colour-coded.

containing either $P_t$ or MPn as the sole P source. We specifically selected *Synechococcus* strain MITS9220 (clade CRD1a representative) associated with mesotrophic environments and strain WH8102 (clade III representative) found in oligotrophic waters, to understand growth physiology for isolates from environments with known differences in $P_i$ availability.

We show both *Synechococcus* strains, MITS9220 and WH8102, when grown in the presence of either $P_t$ or MPn as the sole P source, do not exhibit a clearly defined exponential growth (Fig. 5), as opposed to the growth seen in the presence of $P_i$. It is possible that the *Synechococcus* strains tested may have lost their ability to utilise $P_t$ or MPn due to prolonged exposure to $P_i$-rich media in laboratory cultures. However, this scenario seems unlikely as the genomes of these strains lack currently known $P_t$ or MPn metabolising genes (*ptxD, phnY/phnZ* or C-P lyase). A picocyanobacterial strain with these genes (e.g. *Prochlorococcus* MIT9301) is perfectly able to metabolise $P_t$ and MPn as the sole P source to support its growth [2, 23], despite being in the laboratory cultures for an equivalent amount of time.

For *Synechococcus* MITS9220, beyond day 3, all non-phosphate culture conditions exhibited a steady decline in cell density, reaching an undetectable cell density after day 15, upon which the experiment was terminated for this strain (Fig. 5A). In contrast, while WH8102 did not show exponential growth, it was able to

**Table 2.** Data collection and refinement statistics of MITS9220_PhnD1 structure.

| **Data collection** | | | | |
|---|---|---|---|---|
| Wavelength (Å) | 3.0996 | 2.7552 | 5.166 | 4.8621 |
| Beamline | I23 | I23 | I23 | I23 |
| Resolution (Å) | 106.61–2.02 (2.07–2.02) | 101.2–1.8 (1.84–1.80) | 106.4–3.37 (3.64–3.37) | 106.4–3.39 (3.39–3.17) |
| Space group | C 1 2 1 | C 1 2 1 | C 1 2 1 | C 1 2 1 |
| Unit cell (a, b, c, α, β, γ) | 63.6, 40.7, 106.7, 90, 92.1, 90 | 64.0, 40.7, 101.2, 90, 91.6, 90 | 63.9, 40.7, 106.4, 90, 92.2, 90 | 64.0. 40.8, 106.5 90, 92.2, 90 |
| Total reflections[a] | 384295 (9895) | 884316 (14521) | 14348 (1656) | 17287 (1701) |
| Unique reflections[a] | 18101 (1281) | 24534 (1308) | 3436 (552) | 4119 (578) |
| Multiplicity[a] | 21.2 (7.7) | 36 (11.1) | 4.2 (3) | 4.2 (2.9) |
| Completeness (%)[a] | 99.7 (95.6) | 98.3 (89.3) | 85.1 (67.8) | 85.3 (68.2) |
| Mean I/σ (I)[a] | 40.5 (12.2) | 10.8 (1.1) | 8.8 (5.6) | 13.2 (8.2) |
| $CC_{half}$[a] | 1.000 (0.994) | 0.999 (0.882) | 0.976 (0.939) | 0.989 (0.978) |
| $R_{merge}$[a] | 0.061 (0.113) | 0.185 (1.19) | 0.137 (0.202) | 0.088 (0.116) |
| $R_{meas}$[a] | 0.062 (0.121) | 0.187 (1.246) | 0.158 (0.246) | 0.101 (0.141) |
| $R_{pim}$[a] | 0.012 (0.042) | 0.027 (0.346) | 0.075 (0.137) | 0.047 (0.077) |
| ***Refinement*** | **(PDB: 7S6G)** | | | |
| $R_{factor}/R_{free}$ | 0.155/0.1960 | | | |
| RMSD bonds | 0.0145 | | | |
| RMSD angles | 1.85 | | | |
| *No. of non-H atoms* | | | | |
| Protein | 2129 | | | |
| Ligands | 17 | | | |
| Ions | 10 | | | |
| Water | 256 | | | |
| Protein residues | 273 (1 chain) | | | |
| *Average B-factors* | | | | |
| Main/side chain | 17.1/21.2 | | | |
| Ligands/ions | 30.4/48.5 | | | |
| solvent | 30.6 | | | |
| *Ramachandran* | | | | |
| favoured (%) | 98.17 | | | |
| allowed (%) | 1.1 | | | |
| Molprobity/clash score | 0.72/0.69 | | | |

[a]Values in the parenthesis are for data in the high-resolution outer shell.

**Table 3.** Sequence and structural similarities of MITS9220_PhnD1 with homologous SBPs.

| **Protein** | **Seq. ID (%)** | **PDB** | **r.m.s.d. (Å)** | **Ligand** | **Resolution (Å)** | **Reference** |
|---|---|---|---|---|---|---|
| Pm_PhnD1 | 56 | 5LQ5 | 1.1 | $P_t$ | 1.46 | [13] |
| | | 5LQ8 | 1.1 | MPn | 1.52 | |
| Pm_PtxB (PhnD2) | 30 | 5LV1 | 1.7 | $P_t$ | 2.12 | [13] |
| *T. erythraeum IMS101* PtxB | 27 | 5JVB | 1.6 | $P_t$ | 1.95 | [13] |
| | | 5LQ1 | 1.7 | MPn | 1.41 | |
| *P. stutzeri* PtxB | 32 | 5O2J | 1.9 | $P_t$ | 1.52 | [13] |
| | | 5O37 | 2.0 | MPn | 1.37 | |
| | | 5O2K | 5.1 | no ligand | 2.10 | |
| Ec_PhnD | 22 | 3P7I | 2.4 | 2-AEP | 1.7 | [62] |
| | | 3QUJ | 2.4 | unknown ligand | 2.2 | |
| *P. aeruginosa* PhnD | 21 | 3N5L | 2.3 | Unknown | 1.97 | n/a |
| *C. arsenatis* ArrX | 22 | 6X6B | 2.4 | Sulphate | 1.67 | [63] |
| | | 6XL2 | 2.5 | Arsenate | 1.74 | |
| | | 6XAD | 2.6 | Formate | 1.89 | |
| | | 6XAB | 2.7 | Acetate | 1.78 | |
| | | 6X9G | 3.1 | Malonate | 1.68 | |

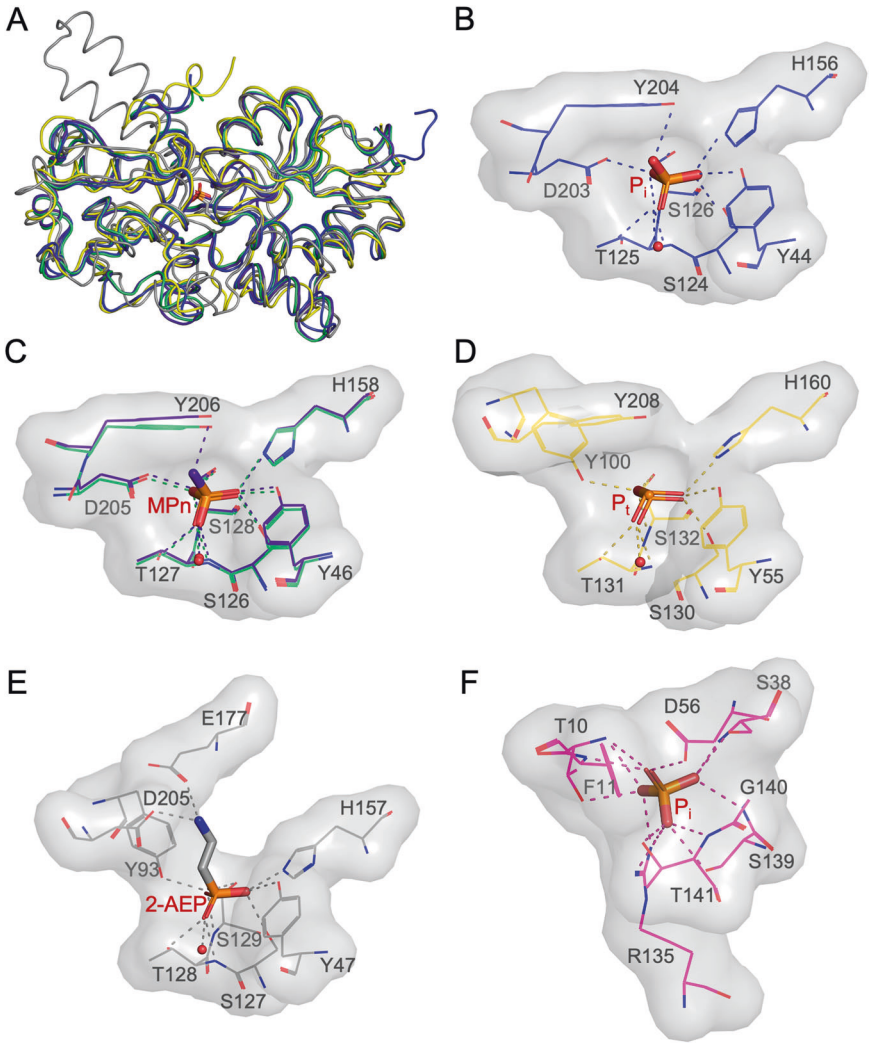


**Fig. 4 Comparison of MITS9220_PhnD1 protein structure with structural homologues. A** The overlay of the crystal structure of *Synechococcus* MITS9220_PhnD1 in complex with $P_i$ (blue; PDB 7S6G), *Prochlorococcus* MIT9301_PhnD1 (green; PDB 5LQ5) and MPn (purple; PDB 5LQ8), *Prochlorococcus* MIT9301_PhnD2 (yellow; PDB 5LV1). The ligand binding cavity (grey surface) with side-chain and ligand interactions is depicted for (**B**) *Synechococcus* MITS9220_PhnD1 in complex with $P_i$, (**C**) *Prochlorococcus* MIT9301_PhnD1 and MPn, (**D**) *Prochlorococcus* MIT9301_PhnD2, (**E**) *E. coli* PhnD in complex with 2-AEP (grey; PDB 3P7I) and (**F**) *E. coli* PstS in complex with $P_i$ (pink; PDB 2ABH).

persist for much longer, with detectable cell densities measured for all culture conditions for the entire duration of the experiment (49 days; Fig. 5B). It is unclear from our growth data if the observed persistence of WH8102 in P-deplete conditions is a result of the strain's capability to persist in nutrient-deplete oligotrophic conditions or if they perhaps can support biotic (via unknown enzymatic pathways) or abiotic conversion of $P_t$ or Pn to $P_i$. A recent study in *E. coli* demonstrated that in the absence of the two known canonical $P_i$ transport-related genes that were sequentially deleted, the Phn uptake system could support growth with $P_i$ as the sole P source [38].

## CONCLUSIONS

All picocyanobacteria strains encode a well-conserved predicted ABC transporter, PhnDCE, that has long been thought to provide a competitive advantage in nutrient deplete conditions. We (for *Synechococcus* isolates) and others (for *Prochlorococcus* isolates) have successfully shown that the PhnD1 protein has a high-affinity for $P_t$ and a medium-affinity for $P_i$ and MPn. However, most picocyanobacterial strains lack known phosphite degradation or C-P lyase pathways to metabolise $P_t$ or MPn. Our findings show that the PhnD1 expression and abundance in the global oceans is not influenced by the phosphate concentration. We further demonstrate the inability of several picocyanobacterial strains (including *Synechococcus* WH8102 and MITS9220 in this study) to grow on $P_t$ or MPn as a sole P source. Taken together, these findings suggest that the PhnDCE system may function as a constitutive $P_i$ transporter.

None of the *Synechococcus* PhnD1 proteins under investigation displayed a measurable affinity for hypophosphite, implying the requirement for minimally three covalently bound oxygen atoms in a trigonal arrangement to engage specific protein sidechains. Our structure of MITS9220_PhnD1 in complex with $P_i$ shows an extensive H-bond network with $P_i$. However, they are fewer than the hydrogen bond interactions in the high-affinity PstS protein with $P_i$ (e.g. in *E. coli*). This explains the lower measured affinity of picocyanobacterial PhnD1 proteins to $P_i$ with a broader substrate range, which may be fortuitous.

We propose two potential scenarios that explain the critical role of PhnD1 in the environment. First, it is likely that PhnD1 aids in the recycling of phospholipid polar headgroups via a predicted

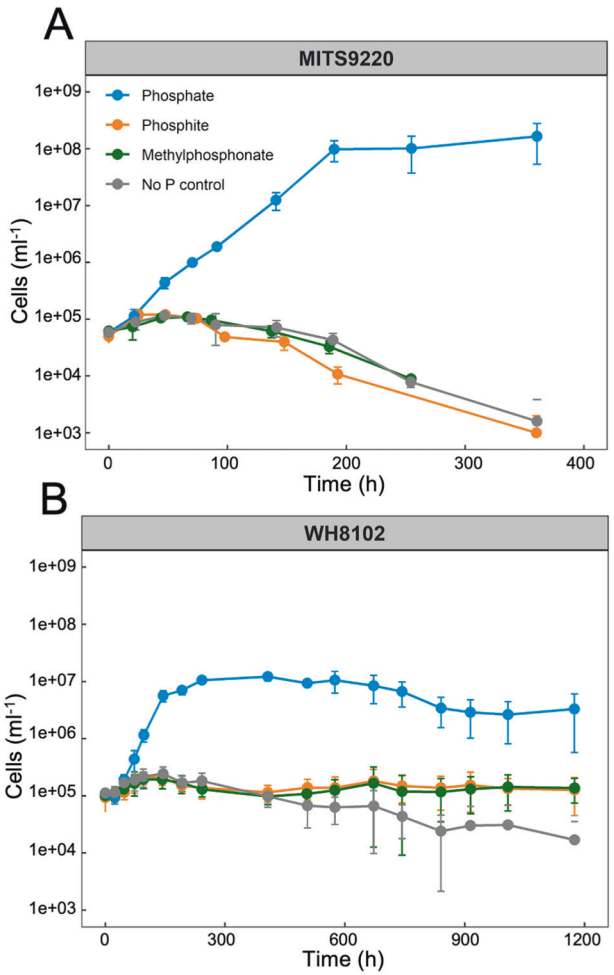


**Fig. 5 Growth curves of *Synechococcus* MITS9220 and WH8102 in the presence of various P sources as the sole P source.** *Synechococcus* MITS9220 (**A**) and WH8102 (**B**) do not support well-defined exponential growth in the presence of $P_t$ or MPn as a sole P source. The cultures were grown in PCR-S11 medium containing $P_i$ (blue), $P_t$ (orange), and MPn (green) in addition to the no P control (grey). The cell density was measured at regular intervals using a CytoFLEX S flow cytometer. The standard deviation of the mean cell density from triplicate cultures is represented as error bars.

phospholipase encoded by *tesA*, which is located adjacent to the *phnDCE* genes. TesA could potentially hydrolyse the commonly found picocyanobacterial phospholipid (PG) to diacylglycerol and glycerol-3-phosphate. Subsequently, the periplasmic alkaline phosphatase would release $P_i$, which can then be taken up by the $PhnD_1CE$ (or Pst) transporter, providing a mechanism for recycling P from the phospholipid bilayer. The second scenario is based on the rate-affinity trade-off that cells mitigate by having multiple transporters for the same nutrient. A medium-affinity $P_i$ transporter such as the $PhnD_1CE$, with potentially fast transport rates, could help picocyanobacterial cells to acquire large amounts of $P_i$ when it is transiently available. This would enable picocyanobacterial cells to balance their requirement for quick transport during sporadic abundance with efficient utilisation of P resources (via Pst transport system) under typical phosphate-deplete conditions.

## MATERIALS AND METHODS

### Genomic and Phylogenetic analyses

Phylogenetic analysis of gene cluster CK_860 annotated as PhnD1 (phosphate/phosphonate-binding proteins) within the Cyanorak database (www.sb-roscoff.fr/cyanorak) [6, 20], was performed using a modified method given by Wilding et al. [39]. Briefly, the 97 orthologous PhnD1 sequences, as well as PhnD2 (CK_6203, 10 sequences) and PhnD3 (CK_56876, 1 sequence), were used to compute a multiple sequence alignment using the L-iNS-I option of MAFFT [40]. The phylogenetic tree was inferred using IQ-Tree [41], using the -TESTONLY option, found to be WAG + G4. The final phylogenetic tree was generated from the inferred and visualised using iTOL [42].

The geographic distribution and expression of PhnD1 and PhnD2 homologues in marine picocyanobacterial populations were analysed using the metagenomes and metatranscriptomes available from the Ocean Microbial Reference Gene Catalogue (OM-RGC) [21, 22]. The protein sequence of *Prochlorococcus* MIT9301_PhnD1 and MIT9301_PhnD2 were used to search against the 'OM_RGC_v2_metaG' and 'OM_RGC_v2_metaT' catalogue using the default parameters. To limit our analyses to picocyanobacterial sequences, we chose a high significance E-threshold ($>e^{-75}$) and ensured that the homologue matches (with sequence identity >70%) for the PhnD1 and PhnD2 sequences did not overlap. Plots were viewed using P as the environmental variable of interest. Additionally, for comparison, we provide environmental abundance maps for *Prochlorococcus* and *Synechococcus* lineage-specific genes. The protein sequence of a predicted chlorophyll b synthase, PcCAO (CK_2331), specific to *Prochlorococcus* strains and a predicted phycocyanin lyase, CpcS (CK_1523), specific to *Synechococcus* strains were used to search against the 'OM_RGC_v2_metaG' catalogue using the default parameters with a high significance E-threshold ($>e^{-75}$).

### Recombinant expression and protein purification

The protein sequences of CC9311_01670, CC9605_01294, MITS9220_01173, and WH8102_01170, annotated to encode PhnD1, were analysed using the SignalP 4.0 [43].

Following truncation of the N-terminal signal peptide (Supplementary Table S3), the genes were PCR-amplified from respective genomic DNA (extracted using the CTAB/phenol-chloroform method) incorporating vector-specific (pOPINF) [44] overhang regions for heterologous expression in *E. coli*. Ligation-independent cloning (Clontech) [45] into the pOPINF vector was carried out using *Kpn*I and *Hin*dIII restriction sites to incorporate an N-terminal hexahistidine tag with a 3C protease cleavage site.

Following plasmid transformation in *E. coli*, all target proteins were expressed to high density using the autoinduction method [46] in a 1 L culture medium. While CC9311_PhnD1, MITS9220_PhnD1, and WH8102_PhnD1 proteins displayed the highest expression in an *E. coli* Lemo strain (BL21 derivative, NE Biolabs), CC9605_PhnD1 achieved higher expression in BL21 derivative strain (Rosetta 2, Novagen). All four PhnD1 proteins were purified using IMAC, as described earlier [47]. Protein-containing fractions were pooled and desalted using size exclusion chromatography (SEC) with a Superdex HiLoad 200 16/600 column (GE Healthcare) equilibrated in buffer containing HEPES (50 mM, pH 7.4), NaCl (300 mM), and glycerol (5% v/v). All buffers contained the reducing agent tris(2-carboxyethyl)phosphine (TCEP, 0.5 mM).

For CC9605_PhnD1, MITS9220_PhnD1, and WH8102_PhnD1 proteins, SEC traces show a single, well-defined peak corresponding to a monomeric state at expected molecular size (~30 kDa). However, for the CC9311_PhnD1 protein, multiple peaks were observed during SEC. Isolation of pure CC9311_PhnD1 occurred by fractionating the peak corresponding to the monomeric species, allowing >90% purity.

### PhnD1 ligand screening and determination of binding affinity to P sources

Ligand screening was performed using differential scanning fluorimetry (DSF) [48] with SYPRO Orange dye (Invitrogen) used to monitor fluorescence at 590 nm following excitation at 485 nm. DSF measures the thermal stability of the protein-ligand complexes, whereby the temperature at which the protein denatures (melting temperature $T_M$) is shifted to a higher temperature in the presence of a stabilising ligand. The compounds that stabilise the protein the most can then be identified as putative ligands for further binding affinity analysis. Compounds tested incorporated cocktails of common protein stabilising ligands (HR2-096 Silver Bullets, Hampton Research) and single-molecule P sources: phosphate, phosphite, hypophosphite, and methyl phosphonate (each as sodium salts). Each condition was tested in triplicate, with each plate containing a control well with no additive. Thermal melt curves were analysed using the analysis template provided [48] and fitting of Boltzmann distribution (GraphPad Prism) to determine mid-point thermal melt temperatures. Cocktail conditions leading to ≥5 °C in melting temperature ($T_M$) were considered a significant increase and repeated in triplicate. The thermal melting curve for all four PhnD proteins,

CC9311_PhnD, CC9605_PhnD, MITS9220_PhnD and WH8102_PhnD, showed a single transition point with a melting temperature ($T_M$) of 47 °C, 32 °C, 46 °C, and 35 °C, respectively.

To elucidate the affinity of PhnD1 to P, the DSF assay was modified and carried out with increasing ligand concentrations as previously described [47], leading to an incremental shift in observed melting temperatures. Data were processed using the provided Python package [29]. Results were plotted and checked for consistency by independently determining $EC_{50}$ values (GraphPad Prism). The standard error of derived $K_D$ values was determined by comparing the deviation in fitting three individual replicates. It was, in all cases, smaller than 10% of the determined affinity measurement.

### MITS9220_PhnD1 crystallisation and structure determination

All four *Synechococcus* PhnD1 purified protein products were subjected to sparse matrix crystallisation screening at 20 °C by sitting drop vapour diffusion method by mixing 0.1 µL of protein (10 mg/mL) with 0.1 µL of the reservoir. However, only MITS9220_PhnD1 showed good diffraction-quality crystals grown in 0.1 M Tris pH 8.5, 25% PEG 3350. Before plunge freezing in liquid nitrogen, MITS9220_PhnD1 crystals were cryo-protected in the mother liquor with an additional 30% (v/v) ethylene glycol. The crystals were further transferred into the vacuum vessel using an adapted cryotransfer system (Leica VCT100).

The data were collected at the Diamond Light Source I23 beamline [49], equipped with the semi-cylindrical Pilatus 12 M (Dectris AG, Switzerland) detector, at four different wavelengths, 2.7552, 3.0996, 4.8621 and 5.1666 Å. Data were processed using XDS [50] and merged using XSCALE. The structure of MITS9220_PhnD1 was solved by experimental phasing using the SAD dataset collected at 3.0996 Å wavelength using the CRANK2 pipeline [51]. After density modification, automated model building within the CRANK2 pipeline produced an initial model comprising a single copy. Several rounds of manual model building and refinement were carried out in COOT [52]and Refmac5 [53] before validating the final model with Molprobity [54]. The final coordinates contain residues 1–270 of the SignalP truncated mature sequence in one chain, with one defined phosphate site, nine chloride anions and three EDO molecules. Final refinement statistics are given in Table 2, and coordinates are deposited in the PDB (7S6G). Anomalous difference Fourier from long-wavelength data was generated using ANODE [55]. The positions of anomalous peaks higher than 4.0σ as output by ANODE from datasets both above (2.755 Å) and below the Ca-edge (3.0996 Å) were inspected in COOT [52] to discount these peaks as calcium. The peaks at 3.0996 Å combined with their absence at 4.8621 Å are indicative of chloride ions. To ascertain whether a phosphate or sulphate was present in the ligand site, anomalous difference Fourier maps were compared from data collected above (4.8621 Å) and below (5.1666 Å) the sulphur absorption edge. The strong peak present in both datasets suggests that the ligand contains phosphorus (Supplementary Fig. S8).

### *Synechococcus* MITS9220 and WH8102 growth in the presence of alternate P sources

*Synechococcus* MITS9220 and WH8102 cultures were grown at 22 °C, with 40 µM photons $m^{-2}$ $s^{-1}$ continuous illumination, in an orbital shaker at 100 rpm in acid-washed polycarbonate flasks using Red Sea salt-based PCR-S11 medium [56]. For treatment conditions containing alternative P compounds, 50 µM $NaH_2PO_4$ was replaced with 50 µM phosphite ($Na_2HPO_3{\cdot}5H_2O$) or methylphosphonate. In P-deplete media, an equal volume of water was added instead of a P compound. Experimental cultures were started from mid-logarithmic cultures grown in phosphate-containing PCR-S11 media. A small inoculum (~100 µL) was used to minimise the transfer of phosphate from stock cultures. Four biological replicates were tested for each experimental condition. Growth was regularly monitored via cell counts using a CytoFLEX S flow cytometer. Cells were identified by chlorophyll and phycoerythrin fluorescence the following excitation using a blue laser (488 nm). Phosphate concentration in all treatment conditions was monitored regularly for the duration of the experiments using a Phosphate Colorimetric kit following the manufacturer's instructions (Sigma-Aldrich) with a detection limit of 0.5 µM.

## DATA AVAILABILITY

The structure coordinates for MITS9220_PhnD1 are deposited in the Protein Data Bank (accession code 7S6G). All other study data is included in the article and/or supporting information files.

## REFERENCES

1. White A, Dyhrman S. The marine phosphorus cycle. Front Microbiol. 2013;4:105.
2. Martinez A, Osburne MS, Sharma AK, DeLong EF, Chisholm SW. Phosphite utilization by the marine picocyanobacterium *Prochlorococcus* MIT9301. Environ Microbiol. 2012;14:1363–77.
3. Feingersch R, Philosof A, Mejuch T, Glaser F, Alalouf O, Shoham Y, et al. Potential for phosphite and phosphonate utilization by *Prochlorococcus*. ISME J. 2012;6:827–34.
4. Moore LR, Ostrowski M, Scanlan DJ, Feren K, Sweetsir T. Ecotypic variation in phosphorus-acquisition mechanisms within marine picocyanobacteria. Aquat Micro Ecol. 2005;39:257–69.
5. Scanlan DJ, Ostrowski M, Mazard S, Dufresne A, Garczarek L, Hess WR, et al. Ecological genomics of marine picocyanobacteria. Microbiol Mol Biol Rev. 2009;73:249–99.
6. Doré H, Farrant GK, Guyet U, Haguait J, Humily F, Ratin M, et al. Evolutionary mechanisms of long-term genome diversification associated with niche partitioning in marine picocyanobacteria. Front Microbiol. 2020;11:567431.
7. Tetu SG, Brahamsha B, Johnson DA, Tai V, Phillippy K, Palenik B, et al. Microarray analysis of phosphate regulation in the marine cyanobacterium *Synechococcus* sp. WH8102. ISME J. 2009;3:835–49.
8. Santos-Beneit F. The Pho regulon: a huge regulatory network in bacteria. Front Microbiol. 2015;6:402.
9. Wanner BL, Chang BD. The phoBR operon in *Escherichia coli* K-12. J Bacteriol. 1987;169:5569–74.
10. Gebhard S, Ekanayaka N, Cook GM. The low-affinity phosphate transporter PitA is dispensable for in vitro growth of *Mycobacterium smegmatis*. BMC Microbiol. 2009;9:254.
11. Ilikchyan IN, McKay RM, Zehr JP, Dyhrman ST, Bullerjahn GS. Detection and expression of the phosphonate transporter gene phnD in marine and freshwater picocyanobacteria. Environ Microbiol. 2009;11:1314–24.
12. Martiny AC, Coleman ML, Chisholm SW. Phosphate acquisition genes in *Prochlorococcus* ecotypes: evidence for genome-wide adaptation. Proc Natl Acad Sci USA. 2006;103:12552–7.
13. Bisson C, Adams NBP, Stevenson B, Brindley AA, Polyviou D, Bibby TS, et al. The molecular basis of phosphite and hypophosphite recognition by ABC-transporters. Nat Commun. 2017;8:1746.
14. Zubkov MV, Mary I, Woodward EM, Warwick PE, Fuchs BM, Scanlan DJ, et al. Microbial control of phosphate in the nutrient-depleted North Atlantic subtropical gyre. Environ Microbiol. 2007;9:2079–89.
15. Zwirglmaier K, Jardillier L, Ostrowski M, Mazard S, Garczarek L, Vaulot D, et al. Global phylogeography of marine *Synechococcus* and *Prochlorococcus* reveals a distinct partitioning of lineages among oceanic biomes. Environ Microbiol. 2008;10:147–61.
16. Zwirglmaier K, Heywood JL, Chamberlain K, Woodward EM, Zubkov MV, Scanlan DJ. Basin-scale distribution patterns of picocyanobacterial lineages in the Atlantic Ocean. Environ Microbiol. 2007;9:1278–90.
17. Ahlgren NA, Rocap G. Culture isolation and culture-independent clone libraries reveal new marine *Synechococcus* ecotypes with distinctive light and N physiologies. Appl Environ Microbiol. 2006;72:7193–204.
18. Fuller NJ, Marie D, Partensky F, Vaulot D, Post AF, Scanlan DJ. Clade-specific 16S ribosomal DNA oligonucleotides reveal the predominance of a single marine *Synechococcus* clade throughout a stratified water column in the Red Sea. Appl Environ Microbiol. 2003;69:2430–43.
19. Sohm JA, Ahlgren NA, Thomson ZJ, Williams C, Moffett JW, Saito MA, et al. Co-occurring *Synechococcus* ecotypes occupy four major oceanic regimes defined by temperature, macronutrients and iron. ISME J. 2016;10:333–45.
20. Garczarek L, Guyet U, Dore H, Farrant GK, Hoebeke M, Brillet-Gueguen L, et al. Cyanorak v2.1: a scalable information system dedicated to the visualization and expert curation of marine and brackish picocyanobacteria genomes. Nucleic Acids Res. 2021;49:D667–D76.
21. Villar E, Vannier T, Vernette C, Lescot M, Cuenca M, Alexandre A, et al. The Ocean Gene Atlas: Exploring the biogeography of plankton genes online. Nucleic Acids Res. 2018;46:W289–95.
22. Sunagawa S, Coelho LP, Chaffron S, Kultima JR, Labadie K, Salazar G, et al. Ocean plankton. Struct Funct Glob Ocean Microbiome Sci. 2015;348:1261359.
23. Sosa OA, Casey JR, Karl DM. Methylphosphonate oxidation in *Prochlorococcus* strain MIT9301 supports phosphate acquisition, formate excretion, and carbon assimilation into purines. Appl Environ Microbiol. 2019;85:e00289-19.
24. Martinez A, Tyson GW, Delong EF. Widespread known and novel phosphonate utilization pathways in marine bacteria revealed by functional screening and metagenomic analyses. Environ Microbiol. 2010;12:222–38.
25. Kovacic F, Granzin J, Wilhelm S, Kojic-Prodic B, Batra-Safferling R, Jaeger KE. Structural and functional characterisation of TesA - a novel lysophospholipase A from *Pseudomonas aeruginosa*. PLoS One. 2013;8:e69125.
26. Van Mooy BA, Fredricks HF, Pedler BE, Dyhrman ST, Karl DM, Koblizek M, et al. Phytoplankton in the ocean use non-phosphorus lipids in response to phosphorus scarcity. Nature. 2009;458:69–72.

27. Simockova M, Holic R, Tahotna D, Patton-Vogt J, Griac P. Yeast Pgc1p (YPL206c) controls the amount of phosphatidylglycerol via a phospholipase C-type degradation mechanism. J Biol Chem. 2008;283:17107–15.
28. Niebling S, Burastero O, Burgi J, Gunther C, Defelipe LA, Sander S, et al. FoldAffinity: binding affinities from nDSF experiments. Sci Rep. 2021;11:9572.
29. Bai N, Roder H, Dickson A, Karanicolas J. Isothermal analysis of ThermoFluor data can readily provide quantitative binding affinities. Sci Rep. 2019;9:2650.
30. Gomez-Garcia MR, Davison M, Blain-Hartnung M, Grossman AR, Bhaya D. Alternative pathways for phosphonate metabolism in thermophilic cyanobacteria from microbial mats. ISME J. 2011;5:141–9.
31. Fukami-Kobayashi K, Tateno Y, Nishikawa K. Domain dislocation: a change of core structure in periplasmic binding proteins in their evolutionary history. J Mol Biol. 1999;286:279–90.
32. Scheepers GH, Lycklama ANJA, Poolman B. An updated structural classification of substrate-binding proteins. FEBS Lett. 2016;590:4393–401.
33. Berntsson RP, Smits SH, Schmitt L, Slotboom DJ, Poolman B. A structural classification of substrate-binding proteins. FEBS Lett. 2010;584:2606–17.
34. Holm L. Dali server: structural unification of protein families. Nucleic Acids Res. 2022;50:W210–5.
35. Yao N, Ledvina PS, Choudhary A, Quiocho FA. Modulation of a salt link does not affect binding of phosphate to its specific active transport receptor. Biochemistry. 1996;35:2079–85.
36. Luecke H, Quiocho FA. High specificity of a phosphate transport protein determined by hydrogen bonds. Nature. 1990;347:402–6.
37. Montano-Gutierrez LF, Correia K, Swain PS. Multiple nutrient transporters enable cells to mitigate a rate-affinity tradeoff. PLoS Comput Biol. 2022;18:e1010060.
38. Stasi R, Neves HI, Spira B. Phosphate uptake by the phosphonate transport system PhnCDE. BMC Microbiol. 2019;19:79.
39. Wilding M, Peat TS, Kalyaanamoorthy S, Newman J, Scott C, Jermiin LS. Reverse engineering: transaminase biocatalyst development using ancestral sequence reconstruction. Green Chem. 2017;19:5375–80.
40. Katoh K, Standley DM. MAFFT multiple sequence alignment software version 7: improvements in performance and usability. Mol Biol Evol. 2013;30:772–80.
41. Nguyen LT, Schmidt HA, von Haeseler A, Minh BQ. IQ-TREE: a fast and effective stochastic algorithm for estimating maximum-likelihood phylogenies. Mol Biol Evol. 2015;32:268–74.
42. Letunic I, Bork P. Interactive Tree Of Life (iTOL) v4: recent updates and new developments. Nucleic Acids Res. 2019;47:W256–W9.
43. Petersen TN, Brunak S, von Heijne G, Nielsen H. SignalP 4.0: discriminating signal peptides from transmembrane regions. Nat Methods. 2011;8:785–6.
44. Berrow NS, Alderton D, Sainsbury S, Nettleship J, Assenberg R, Rahman N, et al. A versatile ligation-independent cloning method suitable for high-throughput expression screening applications. Nucleic Acids Res. 2007;35:e45.
45. Aslanidis C, de Jong PJ. Ligation-independent cloning of PCR products (LIC-PCR). Nucleic Acids Res. 1990;18:6069–74.
46. Studier FW. Protein production by auto-induction in high density shaking cultures. Protein Expr Purif. 2005;41:207–34.
47. Ford BA, Ranjit P, Mabbutt BC, Paulsen IT, Shah BS. ProX from marine *Synechococcus* spp. show a sole preference for glycine-betaine with differential affinity between ecotypes. Environ Microbiol. 2022;24:6071–85.
48. Niesen FH, Berglund H, Vedadi M. The use of differential scanning fluorimetry to detect ligand interactions that promote protein stability. Nat Protoc. 2007;2:2212–21.
49. Wagner A, Duman R, Henderson K, Mykhaylyk V. In-vacuum long-wavelength macromolecular crystallography. Acta Crystallogr D Struct Biol. 2016;72:430–9.
50. Kabsch W. XDS. Acta Crystallogr D Biol Crystallogr. 2010;66:125–32.
51. Pannu NS, Waterreus WJ, Skubak P, Sikharulidze I, Abrahams JP, de Graaff RA. Recent advances in the CRANK software suite for experimental phasing. Acta Crystallogr D Biol Crystallogr. 2011;67:331–7.
52. Emsley P, Cowtan K. Coot: model-building tools for molecular graphics. Acta Crystallogr D Biol Crystallogr. 2004;60:2126–32.
53. Murshudov GN, Skubak P, Lebedev AA, Pannu NS, Steiner RA, Nicholls RA, et al. REFMAC5 for the refinement of macromolecular crystal structures. Acta Crystallogr D Biol Crystallogr. 2011;67:355–67.
54. Chen VB, Arendall WB 3rd, Headd JJ, Keedy DA, Immormino RM, Kapral GJ, et al. MolProbity: all-atom structure validation for macromolecular crystallography. Acta Crystallogr D Biol Crystallogr. 2010;66:12–21.
55. Thorn A, Sheldrick GM. ANODE: anomalous and heavy-atom density calculation. J Appl Crystallogr. 2011;44:1285–7.
56. Rippka R, Coursin T, Hess W, Lichtle C, Scanlan DJ, Palinska KA, et al. *Prochlorococcus* marinus Chisholm et al. 1992 subsp. pastoris subsp. nov. strain PCC 9511, the first axenic chlorophyll a2/b2-containing cyanobacterium (Oxyphotobacteria). Int J Syst Evol Microbiol. 2000;50:1833–47.
57. Sunagawa S, Acinas SG, Bork P, Bowler C, Acinas SG, Babin M, et al. Tara Oceans: towards global ocean ecosystems biology. Nat Rev Microbiol 2020;18:428–45.
58. Belisle BS, Avila Paz AA, Carpenter AR, Cormier TC, Lewis AJ, Menin LS, et al. Genome sequences of *Synechococcus* sp. Strain MITS9220 and cocultured cyanophage SynMITS9220M01. Microbiol Resour Announc. 2020;9:e00481-20.
59. Ahlgren NA, Belisle BS, Lee MD. Genomic mosaicism underlies the adaptation of marine *Synechococcus* ecotypes to distinct oceanic iron niches. Environ Microbiol. 2020;22:1801–15.
60. Rocap G, Distel DL, Waterbury JB, Chisholm SW. Resolution of *Prochlorococcus* and *Synechococcus* ecotypes by using 16S-23S ribosomal DNA internal transcribed spacer sequences. Appl Environ Microbiol. 2002;68:1180–91.
61. Rizk SS, Cuneo MJ, Hellinga HW. Identification of cognate ligands for the Escherichia coli phnD protein product and engineering of a reagentless fluorescent biosensor for phosphonates. Protein Sci. 2006;15:1745–51.
62. Alicea I, Marvin JS, Miklos AE, Ellington AD, Looger LL, Schreiter ER. Structure of the *Escherichia coli* phosphonate binding protein PhnD and rationally optimized phosphonate biosensors. J Mol Biol. 2011;414:356–69.
63. Poddar N, Badilla C, Maghool S, Osborne TH, Santini JM, Maher MJ. Structural and functional investigation of the periplasmic Arsenate-binding protein ArrX from *Chrysiogenes arsenatis*. Biochemistry 2021;60:465–76.

## ACKNOWLEDGEMENTS

This research was supported, in part, by the Australian Research Council Discovery grant (DP200102944) and the Australian Research Council Centre of Excellence in Synthetic Biology (CE200100029) to ITP; BAF acknowledges receipt of an Australian Government Research Training Program (RTP) Scholarship. The authors thank Dr Lisa Moore and Dr Martin Ostrowski for insightful discussions during the course of the research project.

## AUTHOR CONTRIBUTIONS

BSS and ITP designed the experiments and directed the study. BSS, BAF and DV performed laboratory work. BSS and HM performed crystallisation; BSS, HM, CO, and VM collected x-ray data sets and determined protein structure. RJO contributed to the experimental workflows. BSS analysed data; BSS, BAF and ITP wrote the paper. ITP contributed to the funding. All authors contributed to the revisions.

## FUNDING

Open Access funding enabled and organized by CAUL and its Member Institutions.

## COMPETING INTERESTS

The authors declare no competing interests.

## ADDITIONAL INFORMATION

**Supplementary information** The online version contains supplementary material available at https://doi.org/10.1038/s41396-023-01417-w.

**Correspondence** and requests for materials should be addressed to Bhumika S. Shah or Ian T. Paulsen.